CrystEngComm

Twin suppression effect of dihydroxy-benzene isomers during the secondary growth of b-oriented zeolite MFI nanosheet films

Journal:	*CrystEngComm*
Manuscript ID	CE-COM-10-2022-001407.R2
Article Type:	Communication
Date Submitted by the Author:	13-Mar-2023

Complete List of Authors:	Xu, Ruilan; Nanchang Institute of Technology, Nanchang Key Laboratory of Photoelectric Conversion and Energy Storage Materials, College of Science Peng, Yong; Nanchang Institute of Technology, Nanchang Key Laboratory of Photoelectric Conversion and Energy Storage Materials, College of Science; Johns Hopkins University, Department of Chemical and Biomolecular Engineering, Institute for NanoBioTechnology Lu, Peng; Johns Hopkins University, Department of Chemical and Biomolecular Engineering, Institute for NanoBioTechnology Miao, Yurun; Johns Hopkins University, Department of Chemical and Biomolecular Engineering, Institute for NanoBioTechnology Duan, Xuekui; University of Minnesota Twin Cities, Department of Chemical Engineering and Materials Science Lee, Dennis; Johns Hopkins University, Department of Chemical and Biomolecular Engineering, Institute for NanoBioTechnology Wang, Rui; Nanchang Institute of Technology, NanchNanchang Key Laboratory of Photoelectric Conversion and Energy Storage Materials, College of Science Wang, Zhengbao; Zhejiang University, College of Chemical and Biological Engineering Tsapatsis, Michael; Johns Hopkins University, Department of Chemical and Biomolecular Engineering, Institute for NanoBioTechnology; Johns Hopkins University, Applied Physics Laboratory

CrystEngComm

COMMUNICATION

Twin suppression effect of dihydroxy-benzene isomers during the secondary growth of *b*-oriented zeolite MFI nanosheet films

Received 00th January 20xx,
Accepted 00th January 20xx

DOI: 10.1039/x0xx00000x

Ruilan Xu,[a] Yong Peng,*[a,b] Peng Lu,[b] Yurun Miao,[b] Xuekui Duan,[c] Dennis T. Lee,[b] Rui Wang,[a] Zhengbao Wang*[d] and Michael Tsapatsis*[b,e]

The presence of MFI twin crystals on *b*-axis oriented zeolite MFI nanosheet films was suppressed by adding dihydroxy-benzene isomers in the synthesis mixture. The resulting nanosheet films exhibited good intergrowth and a small grain thickness of 30-45 nm within a relatively short synthesis time (hours). The possible twin suppression mechanisms for the three isomers are discussed.

The development of two-dimensional (2D) materials such as graphene/graphene oxide (GO),[1] MXene,[2] 2D zeolite,[3-6] 2D metal-organic frameworks (MOFs),[7,8] 2D covalent organic frameworks (COFs),[9,10] graphitic carbon nitride (g-C_3N_4)[11,12] has provided great opportunities for the fabrication of 2D films/membranes. By precise manipulation of the composition and microstructure, the 2D films/membranes displayed excellent performance for molecular separations or catalytic reactions.[4-11,13-23] For example, by using thin MFI-type zeolite nanosheets as building blocks,[14] zeolite MFI membrane with extremely high para-/ortho- xylene selectivity (separation factor >10000) can be achieved.[15] In comparison, the separation factor of MFI membrane synthesized from the bulky coffin-shaped MFI seed crystals is hard to exceed 1000.[24-27] These two MFI membranes have similar *b*-out-of-plane orientation structure, that is, the straight pore channels are aligned along the cross-sectional directions.[14,15,24-27] The remarkably improved separation performance is mainly attributed to the utilization of high-aspect-ratio MFI nanosheets with large lateral dimensions (>1 μm) as seed layers, leading to the decrease of non-selective grain boundaries within the membrane layer.[14]

Generally, there are two preparation strategies, i.e., top-down method and bottom-up method, to achieve 2D or thicker MFI nanosheets. The top-down method is based on the exfoliation of multi-lamellar MFI zeolite crystals,[4,28] followed by centrifugation to remove non-exfoliated particles.[29] The obtained products are fragmented 2D MFI nanosheets (thickness of about 3 nm),[30] which means their lateral dimensions are relatively small (in sub-micrometer range) and non-uniform. On the other hand, uniformly sized MFI nanosheets could be prepared via a more recently developed anisotropic etching route with an alkaline solution of tetrapropylammonium hydroxide (TPAOH).[31] The thickness of the obtained nanosheets (about 25 nm), however, is considerably high.

The bottom-up method is realized by a direct hydrothermal growth route.[14] Nanometer-sized (30 nm) MFI crystals were used as seeds, and thin MFI nanosheets were prepared by epitaxial growth on the nanoseeds in the presence of organic structure directing agent (OSDA) bis-1,5-(tripropyl ammonium) pentamethylene diiodide (dC5). Compared with the top-down method, this direct synthesis method can produce micrometer-sized large MFI nanosheets, simultaneously, with thickness down to 5 nm. These large (in lateral dimensions) nanosheets were then deposited on substrates as *b*-oriented seed layers to fabricate high-performance MFI separation membranes towards xylene isomer systems.[14,15] In order to maintain the orientation of nanosheet layers, a gel-free growth method that relies on the sacrifice of the top substrate layer was used for secondary growth. Consequently, the thickness of the resulting membranes was relatively large (1 μm in average). When using the traditional secondary growth method, it was found that the *b*-axis preferred orientation of the nanosheet was quickly lost,[19] due to the generation of MFI nuclei in the presence of TPA^+ OSDA and their attachment onto seed layer. Compared with TPA^+, the employment of TEA^+ as OSDA during secondary growth could guarantee the preservation of *b*-orientation of the

[a] Nanchang Key Laboratory of Photoelectric Conversion and Energy Storage Materials, College of Science, Nanchang Institute of Technology, Nanchang 330099, PR China. E-mail: pengyong@nit.edu.cn
[b] Department of Chemical and Biomolecular Engineering and Institute for NanoBio Technology, Johns Hopkins University, Baltimore, MD 21218, USA. E-mail: tsapatsis@jhu.edu
[c] Department of Chemical Engineering and Materials Science, University of Minnesota, Minneapolis, MN 55455, USA.
[d] College of Chemical and Biological Engineering, Zhejiang University, Hangzhou 310027, PR China. E-mail: zbwang@zju.edu.cn
[e] Applied Physics Laboratory, Johns Hopkins University, Laurel, MD 20723, USA.
Electronic Supplementary Information (ESI) available. See DOI: 10.1039/x0xx00000x

resulting MFI films.[26] However, two or three separated hydrothermal synthesis steps were usually needed, implying that this approach was complicated and time-consuming.[19,32] The thickness of the obtained films was still in the range of hundreds of nanometers, imposing limitations on the achievable flux of guest molecules. Therefore, a facile secondary growth method for preparing thin and *b*-oriented MFI zeolite film is highly desired.

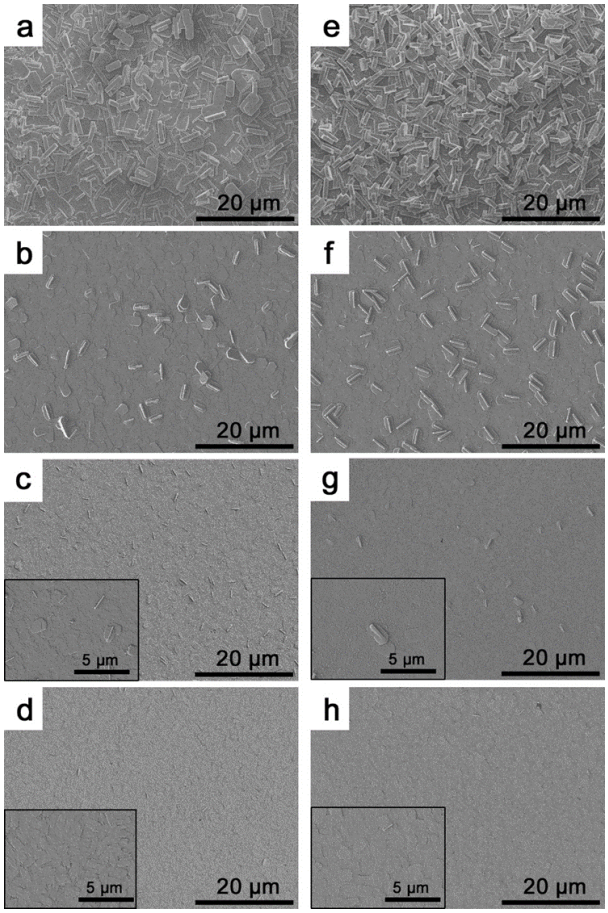

Fig. 1. SEM images of MFI zeolite films synthesized in mixtures with composition: 0.2TPAOH : 1TEOS : 200H_2O : *x*1,3-$C_6H_6O_2$, (a) *x* = 0.1, (b) *x* = 0.3, (c) *x* = 0.6, (d) *x* = 0.8, and the mixtures with composition: 0.2TPAOH : 1TEOS : 200H_2O : *y*1,4-$C_6H_6O_2$, (e) *y* = 0.1, (f) *y* = 0.3, (g) *y* = 1.0, (h) *y* = 1.5.

We previously reported[33,34] that 1,2-dihydroxybenzene (1,2-$C_6H_6O_2$) is a very efficient chelating agent for the complexation of silicate precursor nanoparticles (PNs),[35,36] leading to the achievement of twin-free *b*-oriented MFI zeolite film. It is interesting to see if the isomers of 1,2-$C_6H_6O_2$, 1,3-dihydroxybenzene (1,3-$C_6H_6O_2$) and 1,4-dihydroxybenzene (1,4-$C_6H_6O_2$) can also succeed in eliminating twins, and to determine the applicability of this approach for the fabrication of thin MFI nanosheet films. In this communication, we investigated and compared the twin suppression effect of dihydroxybenzene isomers during secondary growth. *b*-Oriented MFI nanosheet film with grain thickness in the tens of nanometers range was achieved in a relatively short time.

Due to the utilization of MFI nanoseeds, the directly synthesized MFI nanosheets inevitably contain seed nanocrystals embedded at their center.[14] These nanocrystals would probably prevent the accurate observation of twins on nanosheet films. Therefore, we first used uniformly coffin-shaped MFI powders as seed crystals. The procedure is detailed in the ESI. The size of these seeds was about 1 μm (Fig. S1a).[37] Highly *b*-oriented MFI zeolite seed monolayer on stainless steel support was obtained by hand rubbing (Fig. S1b and S1c).[38] It has been confirmed that the film orientation would be randomized in the presence of TPA^+ template during synthesis, and then the twin suppression technique of adding a chelating agent of 1,2-$C_6H_6O_2$ was established.[33,34] Here, we added 1,3-$C_6H_6O_2$ and 1,4-$C_6H_6O_2$ into the synthesis mixtures to make homogeneous mixtures with molar composition of 0.2TPAOH : 1TEOS (tetraethylorthosilicate) : 200H_2O : *x*1,3-$C_6H_6O_2$ and 0.2TPAOH : 1TEOS : 200H_2O : *y*1,4-$C_6H_6O_2$, respectively.

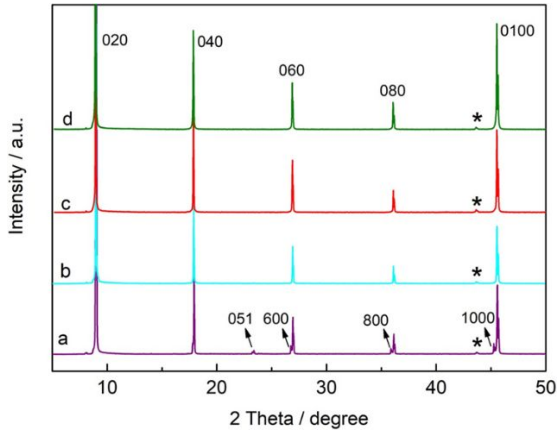

Fig. 2. XRD patterns of MFI zeolite films synthesized in mixtures with composition: 0.2TPAOH : 1TEOS : 200H_2O : *x*1,3-$C_6H_6O_2$, (a) *x* = 0.1, (b) *x* = 0.3, (c) *x* = 0.6, (d) *x* = 0.8. (*) Peaks from the SS plate.

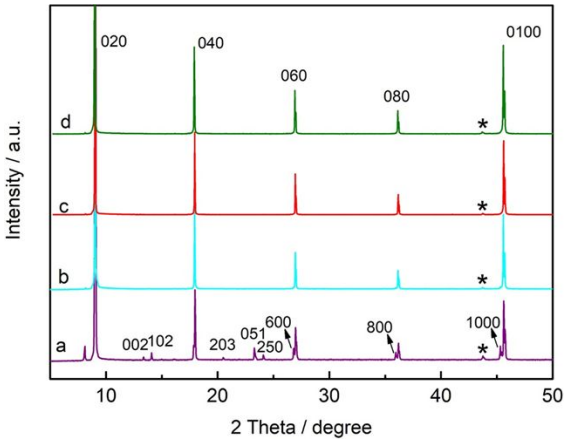

Fig. 3. XRD patterns of MFI zeolite films synthesized in mixtures with composition: 0.2TPAOH : 1TEOS : 200H_2O : *y*1,4-$C_6H_6O_2$, (a) *y* = 0.1, (b) *y* = 0.3, (c) *y* = 1.0, (d) *y* = 1.5. (*) Peaks from the SS plate.

SEM images of the resulting MFI films fabricated on stainless steel supports at 165 °C for 4 h are presented in Fig. 1. It can be clearly observed that there were a lot of MFI twin crystals covering the film layer when the mixture composition is 0.2TPAOH : 1TEOS : 200H_2O : 0.1 1,3-/1,4-$C_6H_6O_2$ (Fig. 1a and 1e). With the increase of $C_6H_6O_2$, the presence of twin crystals attached onto the film surfaces was gradually suppressed. After

optimization, we found that MFI twins can be rarely seen on the film when the mixture composition was 0.2TPAOH : 1TEOS : 200H_2O : x 1,3-$C_6H_6O_2$ with x=0.6 and 0.2TPAOH : 1TEOS : 200H_2O : y 1,4-$C_6H_6O_2$ with y=1 (Fig. 1c and 1g). The thickness of the two films is about 420 nm (see cross-sectional SEM images in the ESI, Fig. S2), which is similar to the film previously synthesized in the presence of 1,2-$C_6H_6O_2$ (thickness of about 440 nm[33]). The obtained films were characterized by X-ray diffraction (Fig. 2 and 3). In the case of the film prepared from *x*=0.1-(1,3)-$C_6H_6O_2$ (Fig. 2a), besides the presence of five (0*k*0) characteristic peaks, i.e., (020), (040), (060), (080), (0100), owing to the *b*-axis out-of-plane orientation in seed monolayers (Fig. S1b and S1c),[37-39] new peaks like (051), (600), (800) and (1000) were observed, which is consistent with the SEM characterization (Fig. 1a). When *x* increased to 0.3 and higher, we can only see (0*k*0) diffraction peaks (Fig. 2b-d), confirming the absence of twins. The progressive elimination of twins is evident by SEM images shown in Fig. 1b-d. Similar XRD patterns were observed for the films achieved by synthesis mixtures with 1,4-$C_6H_6O_2$ (Fig. 3), except for the one from y=0.1-(1,4)-$C_6H_6O_2$. It can be seen from Fig. 3a that many reflections appeared between the (0*k*0) peaks. This is consistent with the SEM image that numerous randomly oriented grains and twins were covering the film surface (Fig. 1e). The films in Fig. 1c and 1g were calcined at 450°C to remove the templates occluded in the zolite channels. SEM and XRD characterizations (see Fig. S3 and S4 in the ESI) for the films did not show obviously change, indicating that the surface morphology and crystal orientation were preserved after calcination.

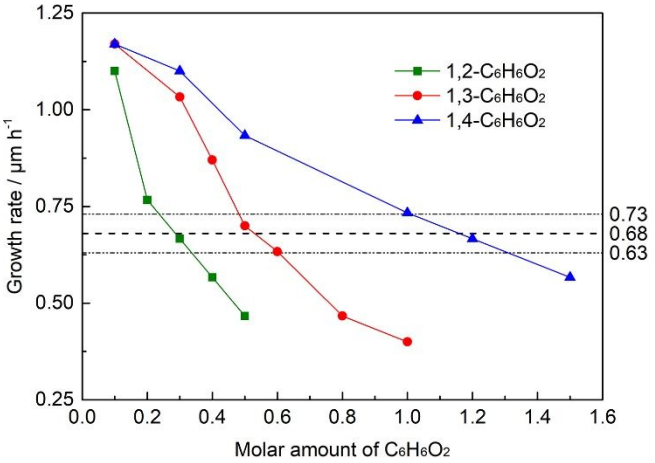

Fig. 4. Crystal growth rate along the *c*-axis of MFI zeolites in the films synthesized with different molar amounts of dihydroxy-benzene isomers, square: 1,2-$C_6H_6O_2$, circle: 1,3-$C_6H_6O_2$, triangle: 1,4-$C_6H_6O_2$. The MFI seed crystal size is 1.0 μm in the *c*-direction. The growth rate was calculated according to the formula of (crystal size - seed size)/(synthesis time - 1)[31]. The lines are used only to show the tendency.

The amount of 1,2-$C_6H_6O_2$ in the mixture with composition 0.2TPAOH : 1TEOS : 200H_2O : 0.3-(1,2)-$C_6H_6O_2$ is sufficient to completely suppress the appearance of twins on the film surface[33] while higher contents are needed for the isomers. To make a better comparison with the twin suppression effect of $C_6H_6O_2$ isomers, we measured the growth rate of crystals along the *c*-axis of MFI in the films synthesized in the mixture of 0.2TPAOH : 1TEOS : 200H_2O : (0~1.5)$C_6H_6O_2$ for all the isomers. The results are plotted in Fig. 4 (see the corresponding SEM images in the ESI, Fig. S5). It can be seen that the growth rate of the crystal along the *c*-axis direction decreased with the increase of the added amount of $C_6H_6O_2$. Each isomer caused a different level of the decrease in crystal growth rate. The decrease was the fastest for 1,2-$C_6H_6O_2$, followed by 1,3-$C_6H_6O_2$, and the slowest for 1,4-$C_6H_6O_2$. This is consistent with the inhibitory effect of $C_6H_6O_2$ addition on the twin growth of seeds (see Fig. 1 and our previous result[33]). That is to say, reducing the growth rate of the seed crystal can effectively inhibit the growth of twin crystals, and the greater the reduction of the seed crystal growth rate, the stronger the effect of suppressing the growth of twin crystals. Interestingly, no matter which $C_6H_6O_2$ isomer is used, as long as the added amount can control the growth rate in the *c*-axis direction of the crystal at 0.68 ± 0.05 μm h^{-1}, it has a benefitial effect of suppressing twin growth. Based on the results from SEM and XRD as well as the above analysis, the synthesis mixtures with molar composition of 0.2TPAOH : 1TEOS : 200H_2O : 0.3-(1,2)-$C_6H_6O_2$, 0.2TPAOH : 1TEOS : 200H_2O : 0.6-(1,3)-$C_6H_6O_2$, and 0.2TPAOH : 1TEOS : 200H_2O : 1.0-(1,4)-$C_6H_6O_2$ were identified as the suitable composition for twin suppression and, therefore, were utilized for preparing thin MFI nanosheet film in the following work.

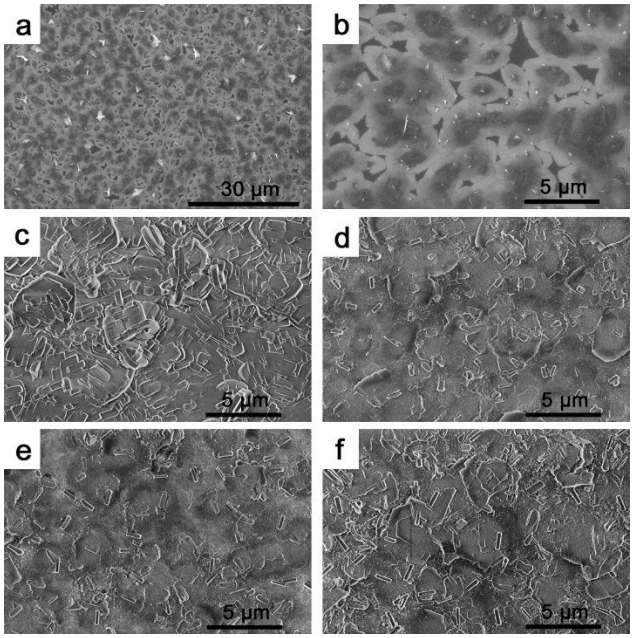

Fig. 5. SEM images of (a, b) MFI nanosheet seed monolayer on silicon wafer and MFI nanosheet films synthesized in mixtures with composition (c) 0.2TPAOH : 1TEOS : 200H_2O, (d) 0.2TPAOH : 1TEOS : 200H_2O : 0.3(1,2-)$C_6H_6O_2$, (e) 0.2TPAOH : 1TEOS : 200H_2O : 0.6(1,3-)$C_6H_6O_2$, and (f) 0.2TPAOH : 1TEOS : 200H_2O : 1.0(1,4-)$C_6H_6O_2$.

MFI nanosheets were prepared by a direct synthesis method using dC5 as a structure-directing agent.[14] A floating-particle coating method was employed to fabricate a nanosheet-seeded monolayer on a silicon wafer.[15] The near rhombus-shaped nanosheets were laid compactly on the support with the largest crystal facet, as can be seen from Fig. 5a and 5b. Nanocrystals

located at the center of the nanosheet came from the original nanoseeds used for the nanosheet preparation. XRD analysis (Fig. 6a) showed that only the (020) reflection can be detected, which was ascribed to the predominant ultra-thin thickness (about 5 nm measured by AFM, see Fig. 7a, for >60% area) of the nanosheet, confirming the *b*-axis preferred orientation of the nanosheet seed layer. MFI nanosheet film was first synthesized in the conventional pure TPA synthesis mixture (0.2TPAOH : 1TEOS : 200H_2O). As shown in Fig. 5c, many new MFI crystals generated in the synthesis mixture were attached on the nanosheet surface and then intergrown as a second layer at the film top. Besides the (0*k*0) reflections, the (501), (600), (800), and (1000) peaks were detected (Fig. 6b), indicating that the *b*-orientation of the zeolite film was compromised. AFM height profile (Fig. 7b) showed a step increase in thickness of an isolated MFI crystal that corresponds to the bottom nanosheet layer of ~ 300 nm to the top new zeolite layer of ~ 400 nm. The overall 700 nm thickness was clearly too high, sacrificing the ultra-thin advantage of MFI nanosheet seeds.

Synthesis mixtures with added 1,2-$C_6H_6O_2$, 1,3-$C_6H_6O_2$, and 1,4-$C_6H_6O_2$ were then used for the secondary growth of MFI nanosheets. The synthesis was carried out at 165°C for 4 h. SEM observations (Fig.5d, e, f) showed that continuous MFI nanosheet films without voids were achieved. A few twin crystals were scattered on film surfaces. Compared with the seed layer, five (0*k*0) reflections were detected by XRD (Fig. 6c, d, e), implying that the nanosheet films were preferentially *b*-axis oriented, despite the appearance of a small (501) peak. We considered that twin crystals sparsely distributed on the nanosheet film came from two sources. Few MFI nuclei generated in the synthesis mixture contributed a small fraction of these twins, as depicted by Fig. 1c and 1g. A major portion of twin crystals should be originated from the nanosheet seeds themselves, because the small nanocrystal embedded at the nanosheet center could also grow. As evidenced from AFM images (Fig. 7c, d, and e), epitaxial growth of 2D nanosheets occurred, accompanied by the formation of twin crystals at the center for all the synthesis compositions after secondary growth. The corresponding height profiles showed that, except for these scattered central twins, most areas of the nanosheets have a thickness ranging from 30 to 45 nm, confirming that we successfully obtained thin MFI nanosheet films by adding $C_6H_6O_2$ isomers in the synthesis mixture. The grain thickness of the nanosheets was used to represent the thickness of nanosheet film.

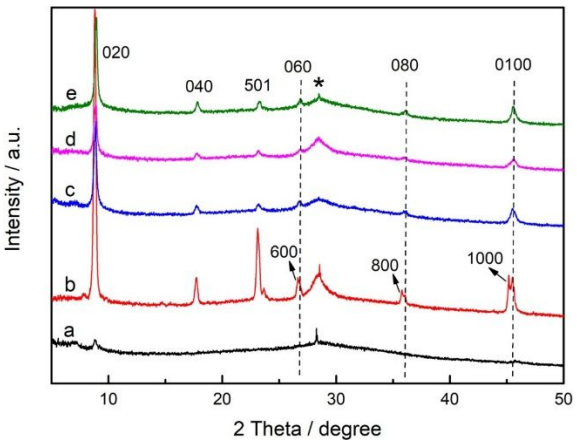

Fig. 6. XRD patterns of (a) MFI nanosheet seed monolayer on silicon wafer and MFI nanosheet films synthesized in mixtures with composition: (b) 0.2TPAOH : 1TEOS : 200H_2O, (c) 0.2TPAOH : 1TEOS : 200H_2O : 0.3(1,2-)$C_6H_6O_2$, (d) 0.2TPAOH : 1TEOS : 200H_2O : 0.6(1,3-)$C_6H_6O_2$, and (e) 0.2TPAOH : 1TEOS : 200H_2O : 1.0(1,4-)$C_6H_6O_2$. (*) Peaks from the silicon wafer.

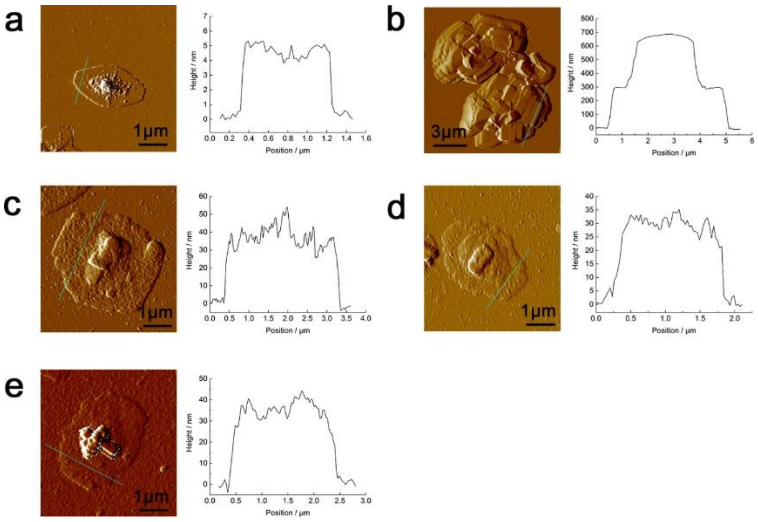

Fig. 7. AFM height images with height profiles along the indicated trace. (a) MFI nanosheet seed on silicon wafer. MFI crystals obtained by growing nanosheets like the one shown in (a), using a mixture with composition (b) 0.2TPAOH : 1TEOS : 200H_2O, (c) 0.2TPAOH : 1TEOS : 200H_2O : 0.3(1,2-)$C_6H_6O_2$, (d) 0.2TPAOH : 1TEOS : 200H_2O : 0.6(1,3-)$C_6H_6O_2$, and (e) 0.2TPAOH : 1TEOS : 200H_2O : 1.0(1,4-)$C_6H_6O_2$ at 165 °C for 4 hrs.

The twin suppression ability of all three $C_6H_6O_2$ isomers during secondary growth for both the seed monolayer of bulky MFI crystals and MFI nanosheets is remarkable. A film formation mechanism based on controlled nutrient release in the presence of 1,2-$C_6H_6O_2$ was proposed in previous work.[33] 1,2-$C_6H_6O_2$ was considered to be a chelating agent, which by complexing with the silicate precursor nanoparticles (PNs) reduces their reactivity and suppresses the formation of twin crystals. The formation of a six-coordinate silicon-1,2-$C_6H_6O_2$ complex was confirmed by the liquid-state ^{29}Si-NMR characterization. A new peak at chemical shift of about -144 ppm appeared in the growth mixture after secondary growth. Here, we performed similar ^{29}Si-NMR experiments for the

growth mixture containing 1,3-$C_6H_6O_2$ and 1,4-$C_6H_6O_2$. However, only a broad peak at around -108.1 ppm was observed, and no new peak could be detected (Fig. S6). To ensure the thorough characterization of the products, the solid gel precipitated at the bottom of the autoclave after secondary growth was further examined by solid-state ^{29}Si-NMR. A new peak at about -141 ppm can be readily observed for the 1,2-$C_6H_6O_2$-containing precipitate (Fig. S7), suggesting again the formation of a silicon complex. We still cannot, however, find any new resonance peak for the precipitate that contains 1,3-$C_6H_6O_2$, even if the scanning time was remarkably extended (Fig. S8). These results suggest that 1,3-$C_6H_6O_2$ and 1,4-$C_6H_6O_2$ could not complex with PNs in the synthesis mixture, probably due to the relatively far distance between the two -OH groups in these molecules. Their twin suppression mechanism could be more analogous to the crystallization-mediating agent of ammonium salts,[35] i.e., silicate-NH_4^+ interactions dominate over silicate-TPA^+ interactions, which will effectively suppress nucleation and slow down the crystal growth rate during secondary growth due to the templating role of TPA^+ in the formation of MFI zeolite nuclei. On one hand, the addition of 0.6-(1,3)-$C_6H_6O_2$ and 1.0-(1,4)-$C_6H_6O_2$ can cause the decrease in pH value of the synthesis mixture (see ESI) to 8.8 and 9.1 from 10.9 (without adding $C_6H_6O_2$ isomers), respectively, slowing down the nucleation and crystallization process. On the other hand, the phenoxy anions after hydrogen ion dissociation would compete with the negatively charged PNs for TPA^+. Due to the introduction of a large amount of phenoxy anions, the number of PNs-TPA^+ complexes, a leading step in the nucleation process, could be significantly reduced. Moreover, the pH of the synthesis mixture after adding 0.3-(1,2)-$C_6H_6O_2$ was also decreased to 9.12. Besides the confirmed chelating effect, we cannot exclude the existence of a crystallization-mediating effect during secondary growth. Then, the two mechanisms may coexist when adding 1,2-$C_6H_6O_2$. The twin suppression mechanism may vary between the three $C_6H_6O_2$ isomers, but eventually, twin crystals on the films were suppressed dramatically by tuning the synthesis compositions.

Compared with gel-free or multi-step or binary-template synthesis approach,[15,19,32] the method developed here is facile and efficient. As far as we know, this is the first report of fabricating highly *b*-oriented MFI nanosheet film with thin grain thickness of tens of nanometers in a short synthesis time of hours. Although twin crystals cannot be eliminated completely, their presence is reduced to a level that can be attributed to the presence of twin seeds in the center of nanosheets. If the aspect ratio of nanosheets could be increased or if a uniformly thin and twin-free nanosheet could be obtained, we can surmise that the number of twins on the nanosheet film would be further reduced. Very recently, the preparation of thickness-improved MFI nanosheets without large nanocrystals was realized by using nanosheet fragments as seeds.[40] Future work should explore using these twin-free MFI nanosheets in combination with the $C_6H_6O_2$ additives towards complete elimination of twins.

Conclusions

In summary, the twin crystal suppression effect of 1,2-$C_6H_6O_2$, 1,3-$C_6H_6O_2$ and 1,4-$C_6H_6O_2$ during the synthesis of MFI zeolite films were comparatively investigated. By using the corresponding optimized protocols, highly *b*-oriented MFI nanosheet films with a grain thickness down to 30-45 nm were successfully achieved for all three $C_6H_6O_2$ isomers. In addition, the twin suppression mechanisms for the $C_6H_6O_2$ isomers were discussed. We believe the efficient synthesis approach reported here would accelerate the fabrication of zeolite nanosheet films/membranes with preferred micro-structure.

Conflicts of interest

There are no conflicts to declare.

Acknowledgements

This work was financially supported by the National Natural Science Foundation of China (21868017 and 21506088), the China Scholarship Council (201908360037), and the U.S. Department of Energy, Office of Science, Office of Basic Energy Sciences, Division of Chemical Sciences, Geosciences and Biosciences under Award No. DE-SC0023403 (Separation Science Program).

References

1 K. S. Novoselov, A. K. Geim, S. V. Morozov, D. Jiang, Y. Zhang, S. V. Dubonos, I. V. Grigorieva and A. A. Firsov, Science, 2004, **306**, 666-669.
2 M. Naguib, M. Kurtoglu, V. Presser, J. Lu, J. Niu, M Heon, L. Hultman, Y. Gogotsi and M. W. Barsoum, Adv. Mater., 2011, **23**, 4248-4253.
3 W. J. Roth, P. Nachtiga, R. E. Morris and J. Čejka, Chem. Rev., 2014, **114**, 4807-4837.
4 K. Varoon, X. Y. Zhang, B. Elyassi, D. D. Brewer, M. Gettel, S. Kumar, J. A. Lee, S. Maheshwari, A. Mittal, C. Y. Sung, M. Cococcioni, L. F. Francis, A. V. McCormick, K. A. Mkhoyan and M. Tsapatsis, Science, 2011, **334**, 72-75.
5 A. Corma, V. Fornes, S. B. Pergher, Th. L. M. Maesen and J. G. Buglass, Nature, 1998, **396**, 353-356.
6 M. Choi, K. Na, J. Kim, Y. Sakamoto, O. Terasaki and R. Ryoo, Nature, 2009, **461**, 246-249.
7 Y. Peng, Y. S. Li, Y. J. Ban, H. Jin, W.M. Jiao, X. L. Liu and W. S. Yang, Science, 2014, **346**, 1356-1359.
8 M. Yue, Y. J. Fu, C. P. Zhang, J. X. Fu, S. Q. Wang and J. W. Liu, Chin. Chem. Lett., 2022, **33**, 3291-3295.
9 H. W. Fan, M. H. Peng, I. Strauss, A. Mundstock, H. Meng and J. Caro, J. Am. Chem. Soc., 2020, **142**, 6872-6877.
10 L. J. Chen, M. C. Huang, B. Chen, C. T. Gong, N. J. Li, H. F. Cheng, Y. Chen, Y. W. Peng and G. D. Xu, Chin. Chem. Lett., 2022, **33**, 2867-2882.
11 S. Bai, X. J. Wang, C. Y. Hu, M. L. Xie, J. Jiang and Y. J. Xiong, Chem. Commun., 2014, **50**, 6094-6097.
12 R. L. Xu, Y. Peng, Materials, 2019, **12**, 2844.
13 L. Ding, Y. Y. Wei, L. B. Li, T. Zhang, H. H. Wang, J. Xue, L. X. Ding, S. Q. Wang, J. Caro and Y. Gogotsi, Nat. Commun., 2018, **9**, 155.
14 M. Y. Jeon, D. Kim, P. Kumar, P. S. Lee, N. Rangnekar, P. Bai, M. Shete, B. Elyassi, H. S. Lee, K. Narasimharao, S. N. Basahel, S. Al-Thabaiti, W.Q. Xu, H. J. Cho, E. O. Fetisov, R. Thyagarajan,

R. F. DeJaco, W. Fan, K. A. Mkhoyan, J. I. Siepmann and M. Tsapatsis, Nature, 2017, **543**, 690-694.
15 D. Kim, M. Y. Jeon, B. L. Stottrup and M. Tsapatsis, Angew. Chem. Int. Ed., 2018, **57**, 480-485.
16 K. V. Agrawal, B. Topuz, T. C. T. Pham, T. H. Nguyen, N. Sauer, N. Rangnekar, H. Zhang, K. Narasimharao, S. N. Basahel, L. F. Francis, C. W. Macosko, S. Al-Thabaiti, M. Tsapatsis and K. B. Yoon, Adv. Mater., 2015, **27**, 3243-3249.
17 H. Zhang, Q. Xiao, X. H. Guo, N. J. Li, P. Kumar, N. Rangnekar, M. Y. Jeon, S. Al-Thabaiti, K. Narasimharao, S. N. Basahel, B. Topuz, F. J. Onorato, C. W. Macosko, K. A. Mkhoyan and M. Tsapatsis, Angew. Chem. Int. Ed., 2016, **55**, 7184-7187.
18 Z. S. Cao, S. X. Zeng, Z. Xu, A. Arvanitis, S. W. Yang, X. H. Gu and J. H. Dong, Sci. Adv., 2018, **4**, eaau8634.
19 B. Min, S. W. Yang, A. Korde, Y. H. Kwon, C. W. Jones and S. Nair, Angew. Chem. Int. Ed., 2019, **58**, 8201-8205.
20 P. Kumar, D. W. Kim, N. Rangnekar, H. Xu, E. O. Fetisov, S. Ghosh, H. Zhang, Q. Xiao, M. Shete, J. I. Siepmann, T. Dumitrica, B. McCool, M. Tsapatsis and K. A. Mkhoyan, Nat. Mater., 2020, **19**, 443-449.
21 W. J. Roth, T. Sasaki, K. Wolski, Y. Song, D. M. Tang, Y. Ebina, R. Ma, J. Grzybek, K. Kałahurska, B. Gil, M. Mazur, S. Zapotoczny and J. Cejka, Sci. Adv., 2020, **6**, eaay8163.
22 W. J. Dai, C. Kouvatas, W. S. Tai, G. J. Wu, N. J. Guan, L. D. Li and V. Valtchev, J. Am. Chem. Soc., 2021, **143**, 1993-2004.
23 P. Lu, S. Ghosh, M. D. de Mello, H. S. Kamaluddin, X. Y. Li, G. Kumar, X. K. Duan, M. Abeykoon, J. A. Boscoboinik, L. Qi, H. Dai, T. Y. Luo, S. Al-Thabaiti, K. Narasimharao, Z. Khan, J. D. Rimer, A. T. Bell, P. Dauenhauer, K. A. Mkhoyan and M. Tsapatsis, Angew. Chem. Int. Ed., 2021, **60**, 19214-19221.
24 Z. P. Lai, G. Bonilla, I. Diaz, J. G. Nery, K. Sujaoti, M. A. Amat, E. Kokkoli, O. Terasaki, R. W. Thompson, M. Tsapatsis and D. G. Vlachos, Science, 2003, **300**, 456-460.
25 Z. P. Lai, M. Tsapatsis and J.P. Nicolich, Adv. Funct. Mater., 2004, **14**, 716-729.
26 T. C. T. Pham, H. S. Kim and K. B. Yoon, Science, 2011, **334**, 1533-1538.
27 N. Rangnekar, N. Mittal, B. Elyassi, J. Caro and M. Tsapatsis, Chem. Soc. Rev., 2015, **44**, 7128-7154.
28 S. Maheshwari, E. Jordan, S. Kumar, F. S. Bates, R. L. Penn, D. F. Shantz and M. Tsapatsis, J. Am. Chem. Soc., 2008, **130**, 1507-1516.
29 K. V. Agrawal, B. Topuz, Z. Y. Jiang, K. Nguenkam, B. Elyassi, L. F. Francis, M. Tapatsis and M. Navarro, AIChE J., 2013, **59**, 3458-3467.
30 P. Kumar, K. V. Agrawal, M. Tsapatsis and K. A. Mkhoyan, Nat. Commun., 2015, **6**, 7128.
31 Y. Liu, W. L. Qiang, T. T. Ji, M. Zhang, M. R. Li, J. M. Lu and Y. Liu, Sci. Adv., 2020, **6**, eaay5993.
32 D. Kim, M. Shete and M. Tsapatsis, Chem. Mater., 2018, **30**, 3545-3551.
33 Y. Peng, R. L. Xu, X. F. Lu, X. D. Jiang and Z. B. Wang, CrystEngComm, 2019, **21**, 4141-4144.
34 Y. Peng and R. L. Xu, J. Mater. Sci., 2020, **55**, 967-975.
35 X. F. Lu, Y. Peng, Z. B. Wang and Y. S. Yan, Chem. Commun., 2015, **51**, 11076-11079.
36 X. M. Li, Y. Peng, Z. B. Wang and Y. S. Yan, CrystEngComm, 2011, **13**, 3657–3660.
37 R. L. Xu and Y. Peng, Ceram. Int., 2018, **44**, 22352-22356.
38 Y. Peng, R. L. Xu, X. D. Jiang, S. Xu and Z. B. Wang, CrystEngComm, 2018, **20**, 4531-4535.
39 Y. Peng, X. F. Lu, Z. B. Wang and Y. S. Yan, Angew. Chem. Int. Ed., 2015, **54**, 5709-5712.
40 D. Kim, S. Ghosh, N. Akter, A. Kraetz, X. K. Duan, G. Gwak, N. Rangnekar, J. R. Johnson, K. Narasimharao, M. A. Malik, S. Al-Thabaiti, B. McCool, J. A. Boscoboinik, K. A. Mkhoyan and M. Tsapatsis, Sci. Adv., 2022, **8**, eabm8162.